doi:10.1038/nature10096

Supplementary Discussion

Doushantuo Formation cap dolostone

In the Yangtze Gorges area of South China, the basal member of the Ediacaran aged Doushantuo Formation consists of a 3-5 m thick cap dolostone, which is in sharp lithological contact with the underlying glaciogenic diamictite of the Nantuo Formation[1]. The cap dolostone has been described in terms of three distinct units[1-3]. Unit C1, at the base, is 1-1.9 m thick. It consists of microcrystalline dolomite that is commonly brecciated, contains localized limestone blocks, tepee-like structures and cavities lined by multiple generations of fringing cement. The middle layer (C2) consists of laminated dolomicrite, is less than 1m thick and contains local 'tepee-like' structures that disrupt laminations at its base. Thinly laminated, silty, limestone and dolomite, 1.5–2 m thick make up the upper layer (C3)[1,2]. The cap is in transitional contact with an overlying package of shales, marls and muddy dolomites, which in total are ~70 m in thick and collectively make up member 2 of the Doushantuo Formation[2,4].

The majority of carbonate phases in the Doushantuo Formation cap from the Yangtze Gorges area show evidence of diagenetic modification[2,3]. For example, microcrystalline dolomites, the most common phase in the cap, has $\delta^{18}O_{PDB}$ values as low as -14‰ that co-vary with $\delta^{13}C_{PDB}$ values[1,3]. Furthermore, parts of the cap dolostone unit are strongly recrystallized, silicified and cut by late stage quartz and calcite filled veins[2,3]. It is worth noting that virtually all cap dolostones around the world share one or more of these features[5].

Highly ^{13}C-depleted carbonates make up a volumetrically minor portion of the cap and have only been identified in 3 different sections of the Doushantuo Formation

that are km's to 10's km apart[3]. This is despite the fact that many of the textures observed in the cap dolostone from the Yangtze Gorges area, that are attributed to methane seepage, are observed in the cap dolostones all over South China and indeed other parts of the world[5,6]. Reported occurrences of highly ^{13}C-depleted carbonates in the Doushantuo Formation include: 1) dark gray to black isopachous calcite found in sheet cracks, fractures, and cavities in the basal part of the cap (C1), 2) microcrystalline limestone clots associated with tepee-like structures in C2, and 3) clotted mosaics in black to dark gray limestone lenses of C3 (ref.1-3).

Cap dolostone samples analysed in this study

Sample 1 Is a slab collected from unit C1 of the cap dolostone at Jiulongwan (see Supplementary Fig. 1 for section location). It consists of fractured dolomicrite hosting two generations of vein filling calcite (Fig. 1; Supplementary Fig. 2 and 4). The first generation of vein fill consists of coarsely crystalline grey calcite with exceptionally low $\delta^{13}C_{PDB}$ values (down to -32‰), that was subject to later fracturing and is cross-cut by a second generation of veins, now filled with coarse white calcite spar (Fig. 1; Supplementary Table 1).

Sample 2 Comes from unit C1 at Huajipo (Supplementary Fig. 1). It consists of an angular dolomicrite block with internal, mm-scale fractures and recrystallized patches now consisting of white calcite. A complex series of calcite (white and grey) and silica fringing cements line the margins of the dolomicrite block (Supplementary Fig. 3). Only dolomicrite from this sample was subject to geochemical analysis in this study.

Sample 3 Is part of a black limestone lens from unit C2 at Huajipo (Supplementary Fig. 1). This samples $\delta^{13}C_{PDB}$ values vary by more than 30‰ at mm-scales[2]

(Supplementary Fig. 5). Textural features include grey or buff coloured layers up to 4 mm thick, containing finer, internal wavy laminations. Most of these layers are sub-parallel to bedding and extend laterally for up to 7 cm (Fig. 1; Supplementary Fig. 2 and 5), but in some areas the layers are disrupted and fragmented. They are composed of partially calcitized, subhedral to euhedral microcrystalline dolomite cemented by silica (Supplementary Fig. 6). Elongate lenses filled with two generations of calcite cements separate dolomicrite layers and enclose fragments (Fig. 1; Supplementary Fig. 2 and 5). Grey, isopachous cement with crystals up to 0.5 mm and $\delta^{13}C_{PDB}$ values as low as -41.7‰ line the margins of cemented lenses, with white calcite spar filling the central parts of larger lenses (Fig. 1; Supplementary Fig. 5 and 6).

Alternative origins of low Δ_{47} values?

The highly ^{13}C-depleted calcite cements from the Doushantuo Formation cap dolostone have the lowest Δ_{47} values of any natural carbonate samples currently known. Here we discuss (and rule out) the possibility that exceptionally low Δ_{47} values of these materials result from the unusual effects of mixing or reaction kinetics on clumped isotope systematics.

Because two-component mixing follows linear vectors in isotopic composition space (e.g., the Cartesian coordinates [$^{13}C^{16}O_3$] vs. [$^{12}C^{18}O^{16}O_2$] vs. [$^{13}C^{18}O^{16}O_2$]), but the stochastic distribution is generally a curved surface in that composition space, mixing can lead to deviations from the stochastic distribution. Effects of this kind have been observed experimentally with CO_2 gas[7], and this phenomenon is generally predictable. To demonstrate the possible impact of the mixing effect on Δ_{47} values, we carried out a calculation with two end-member carbonates, both with ^{13}C-^{18}O ordering equivalent to a measured Δ_{47} of +0.45‰, but differing greatly in $\delta^{13}C$ value. One end-member carbonate

has an isotopic composition close to that measured from dolomicrite powder H2 from cap dolostone sample 3 ($\delta^{13}C_{PDB}$= -9‰ and $\delta^{18}O_{PDB}$= -9‰) while the other end member has a $\delta^{13}C_{PDB}$ value of -90‰ and a $\delta^{18}O_{PDB}$ value of +1‰. A 50:50 physical mixture of the two end members, where no oxygen exchange takes place between carbonate ions, would have a bulk $\delta^{13}C_{PDB}$ of -50‰ and $\delta^{18}O_{PDB}$ of -4‰ (similar to values seen in the most ^{13}C-depleted grey calcite), but a ~0.21‰ lower anomaly in ^{13}C-^{18}O bonds (i.e., corresponding to a measured Δ_{47} of +0.24‰ – similar to the 'hottest' carbonates measured from the cap dolostone). The result of this calculation shows that the very low Δ_{47} values we measured could theoretically result from a physical mixture of isotopically distinct carbonates. Other scenarios are possible, but all require a mixing end member that is similarly extreme in its $\delta^{13}C_{PDB}$. However, several arguments oppose this possibility. Most importantly, there is no evidence, either in our sample or terrestrial carbonates generally, for such extraordinarily low $\delta^{13}C_{PDB}$ carbonate. The lowest $\delta^{13}C_{PDB}$ values of carbonates associated with methane seeps are approximately -65‰ (ref. 8). So, this mixing explanation would require the presence of a cryptic component that is tens of per mil outside of the known range of terrestrial carbonate – an alternative we consider unlikely. Furthermore, the very low $\delta^{13}C_{PDB}$ cements in our samples do not appear to be physical mixtures of multiple domains under the petrographic microscope, in maps of elemental compositions, or in previous mm-scale investigations of $\delta^{13}C_{PDB}$ variability[1,2].

An alternative and even less plausible mixing process one might call on is that the parent water from which these carbonates grew was a mixture of two separate aqueous solutions that contained dissolved inorganic carbon species that differed in $\delta^{13}C_{PDB}$ by ~ 100‰, and that carbonate precipitated out of the mixed solution without any isotopic exchange or re-equilibration. Because at high temperatures (> 200 °C), the isotopic equilibration rate is fast (i.e., of the order of seconds – see Supplementary Fig. 7) we conclude that low Δ_{47} values are not a result of mixing.

Our understanding of kinetic isotope effects generally, and clumped isotope fractionations accompanying various kinetically controlled reactions in particular, is incomplete. Of the diverse natural carbonates that have been measured for their Δ_{47} values, however, only a few deviate from the equilibrium precipitation of inorganic calcite[9]. The only common and well-documented example is speleothems, which often show lower Δ_{47} and higher $\delta^{18}O$ values than predicted for equilibrium precipitation of inorganic calcite[10]. This is suspected to result from kinetic isotope fractionation effects during precipitation by rapid CO_2 degassing and/or crystallisation. Guo et al. developed a quantitative theoretical model of kinetic isotope effects caused by rapid CO_2 degassing in speleothems and suggests that it is a consequence of a kinetic isotope effect associated with dissociation of H_2CO_3 and HCO_3^- releasing CO_2 gas[10]. Even if it was possible for rapid CO_2 degassing from a low $\delta^{13}C$ solution to have occurred in the Doushantuo cap dolostone during formation of the highly ^{13}C-depleted cements, the kinetic effect cannot have driven Δ_{47} values ~ 0.1‰ lower than typical values of marbles (~ 0.35‰, ref. 9) particularly because such a degassing would have occurred at much higher temperatures than CO_2 degassing in speleothems (which would both diminish the amplitude of kinetic isotope effects and promote very rapid re-equilibration of carbonate ions with water). Furthermore, a large Δ_{47} decrease by this mechanism should have been associated with a large $\delta^{18}O$ and $\delta^{13}C$ increase, which is not observed (in fact, the opposite is true for low Δ_{47} carbonates in our samples). While we cannot strictly rule out the possibility of some unknown kinetic isotope effect with systematics that differ from degassing, we are aware of no evidence for such a process and therefore reject it as an interpretation of our results.

Discussion of data from dolomicrite and white calcite spar

The main text focuses on the use of our data in order to determine the origins of highly ^{13}C-depleted calcite. Here, we expand the discussion of geochemical data from dolomicrite and white calcite spar in the cap dolostone and explore the possible implications for the origin and diagenetic history of these phases.

Dolomite is the main mineralogical phase observed in Marinoan cap carbonates globally[11]. The origin of the dolomite is still debated and remains an intriguing problem in its own right (e.g., compare refs. 5, 6 and 11). Although we obtained various types of geochemical data from dolomicrite in the cap dolostone, including novel Δ_{47} data, several lines of evidence suggest that the dolomicrite in our samples has been pervasively altered by post-depositional diagenesis and therefore cannot provide insights into its earlier history. The evidence includes: 1) A Mn/Sr ratio of 30 in dolomicrite from sample 3 at Huajipo (Supplementary Table 2), which is well above the threshold value of 2 typically used as an indicator of diagenetic alteration[12], 2) relatively radiogenic $^{87}Sr/^{86}Sr$ ratios in dolomicrite from both sections compared with contemporaneous cap dolostones from other locations[13] (Supplementary Table 3), 3) $\delta^{18}O_{PDB}$ values ranging from -7.36 to -14.31‰ (Supplementary Table 1), which are below the -5‰ threshold used to distinguish altered Neoproterozoic carbonates[14], and 4) clumped isotope temperatures of between 86 and 156 °C; well above expected depositional temperatures (Supplementary Table 1).

As noted in the main text (see also Supplementary Table 2) all three carbonate phases identified in our samples have radiogenic $^{87}Sr/^{86}Sr$ ratios compared to contemporaneous carbonates from other locations and Mn/Sr ratios well above 2, indicating pervasive diagenetic alteration in the cap[15]. This makes it difficult to determine the stage of alteration at which the dolomicrite acquired its current trace element chemistry. It is possible that trace element signatures of dolomicrite reflect: 1)

exchange with waters during post-depositional lithification and mineral stabilisation, 2) exchange with hydrothermal fluids that also precipitated ^{13}C-depleted calcites, 3) exchange with fluids that also precipitated white calcite spar, or, 4) exchange with fluids that did not produce a readily identifiable carbonate phase in the studied samples. It is notable, however, that all three carbonate phases are distinctive in terms of carbonate clumped temperatures and the $\delta^{18}O_W$ of fluid they precipitated from (see Main Text and Fig. 2). In addition, although Mn/Sr and $^{87}Sr/^{86}Sr$ of all phases are relatively high in comparison with unaltered carbonates, there is still considerable heterogeneity in these ratios between phases (Mn/Sr: dolomicrite = 30, white calcite spar = 89, ^{13}C-depleted grey calcite = 111; Supplementary Figure 4 and 5; Supplementary Table 2 and 3). These observations argue against a single phase of diagenetic alteration resetting all three phases. They also suggest that later fluids precipitating ^{13}C-depleted calcite and white calcite spar did not undergo isotopic or trace element exchange with dolomicrite to any significant degree. This is understandable, in the case of the high temperature hydrothermal episode, given the short duration (hundreds to thousands of years) implied by clay mineral evidence (see Main Text) and the volumetrically minor occurrence of carbonate phases precipitated from hydrothermal fluids in the cap at this stage.

Therefore, we think that dolomicrite may preserve the geochemical signatures of a period of post-depositional lithification and mineral stabilisation. This is supported by the observation that dolomicrite shows a large range in $\delta^{18}O_{PDB}$(from -7.36 to -14.31‰ - PDB) that seems to be correlated with the temperature of crystallisation (with the lowest $\delta^{18}O_{PDB}$ associated with the highest temperatures). Finally, the fact that dolomicrite interacted with fluids with relatively invariant $\delta^{18}O_{SMOW}$ (1±1‰, Fig. 2) indicates an alteration process involving relatively high water-rock ratios.

The latest stage of carbonate precipitation observed in our samples produced white calcite spar filling voids and veins cross-cutting both the dolomicrite and ^{13}C-

depleted calcite. There aren't many constraints that can be put on the timing or origin of the fluid precipitating white calcite spar. But we think this fluid infiltrated the cap after the period of hydrothermalism that produced ^{13}C-depleted calcite (based on petrographic relations), without significant isotopic or chemical exchange with other phases, based on the distinctive temperatures, $\delta^{18}O_{PDB}$ of carbonates and $\delta^{18}O_{SMOW}$ values observed for white calcite spar.

CEC/total clay ratios as a proxy for degree of clay diagenesis

One of the unique properties of clay minerals is that their surfaces often have negative electrostatic charge[16]. The cation exchange capacity (CEC) of different clay minerals varies considerably, and one of the main factors influencing the CEC value of a particular type of clay is if cations in clay interlayers are fixed or exchangeable[16]. All common non-clay minerals have CEC values close to zero, so CEC measured from whole-rock samples comes almost exclusively from clays. As chloritization of saponite occurs, (a typical diagenetic process that requires elevated temperatures) interlayer space becomes fixed with an additional octahedral sheet and the CEC/total trioctahedral clay (chlorite + corrensite + saponite) ratio drops significantly (from ~100 to 10 meq/100g), providing a proxy for the degree of clay diagenesis. The use of this metric is possible because the majority of lower Doushantuo Formation samples only contain clays in the saponite-corrensite-chlorite series[4]. Some samples of the cap dolostone also contain small quantities of illite, but because the CEC of illite is low and varies within a narrow range[16] the contribution of illitic CEC in those samples was easily subtracted from the measured CEC values. Therefore, the corrected CEC/total clay ratios provide a valid indicator of the degree of chloritization in these sections.

Cambrian hydrothermal activity in South China

Evidence for a regionally extensive episode of Cambrian hydrothermal activity in South China is expressed in horizons of synsedimentary polymetallic Ni-Mo-PGE–Au mineralization and associated fluid conduits in zones that extend for 100's of km along the northern and southern margins of the South China Block[17]. Organic-rich black shales host these thin (10's cm scale) mineralized horizons.

Although the enrichment of certain metals is probably linked to scavenging and precipitation from seawater under euxinic conditions, in basins with low rates of sedimentation[18-21], the role of hydrothermal fluids in mineralization is supported by several lines of evidence: 1) a Cambrian aged network of hydrothermal silica-filled chimneys[17], in addition to fluorite and quartz filled stockworks directly beneath horizons enriched in metals[22,23], 2) fluid inclusion data indicating temperatures of up to ~250 °C for fluids flowing through these conduits, with two chemically distinct types of hydrothermal brine recognized[22,23], 3) mineral assemblages in ore beds indicating temperatures of 200-300 °C during the final phase of sulfide/sulfarsenide mineralization[24], 4) petrological evidence of a complex paragenetic history, consistent with compositional evolution and temperature changes of hydrothermal brines[24], and 5) trace element, rare earth element (REE) and Os-isotope evidence for a hydrothermal influence on ore horizons as well as the black-shale host[17,21]. It is hypothesized that the zones of mineralization and remnants of vents are concentrated along the margins of the South China Block because deep-rooted faults in these areas acted as conduits for the migration of fluids to the seafloor[17].

The massive scale of hydrothermalism is indicated not only by the regional extent of the vent fields (with an estimated area of 50,000 to 120,000 km^2 – ref. 17), but also by the coincidence with negative carbon isotope excursions recorded by organic material in

contemporaneous sedimentary rocks. This later observation is hypothesized to be a response to inputs of ^{13}C-depleted carbon from gases like methane released by hydrothermal vents[17]. Given the likely extent of hydrothermal activity in South China during the Cambrian it is not surprising to find evidence of fluid flow in underlying Neoproterozoic sediments, even in areas away from cratonic margins[17]. In fact, some models of ore genesis explicitly hypothesize the circulation of fluids through the Doushantuo Formation[20].

Supplementary Figures

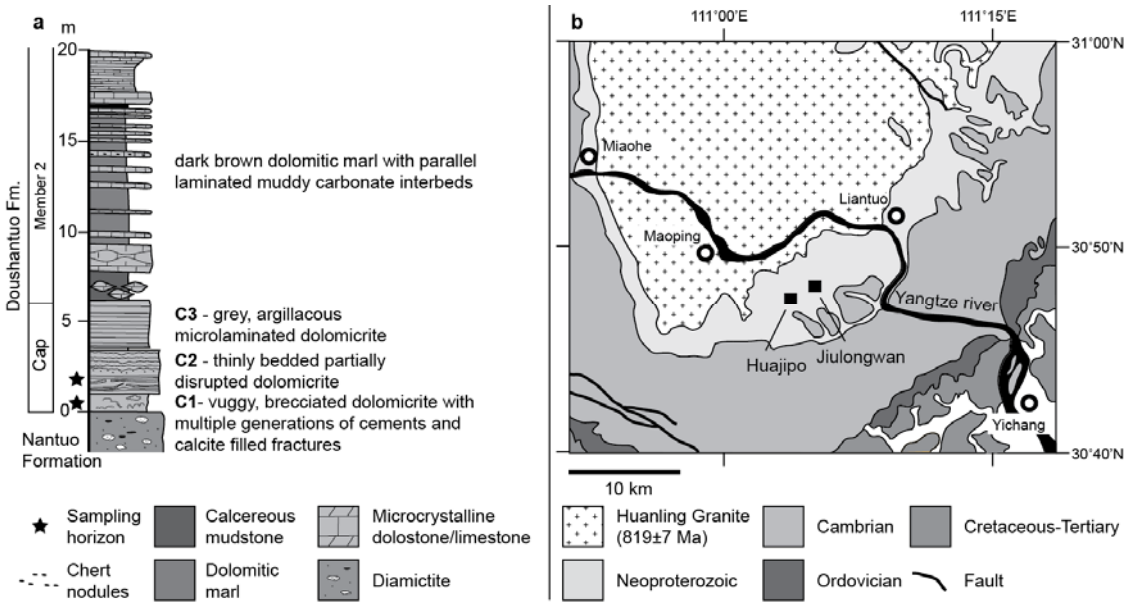

Supplementary Figure 1 | Physical and stratigraphic locations of samples. **a**, stratigraphy of the lower Doushantuo Formation based on a measured section from Jiulongwan, showing the three units C1, C2 and C3 of the cap described in the Supplementary Discussion, following the terminology of refs. 1,2. Sample 1, from Jiulongwan, was collected from unit C1. The Huajipo samples (2 and 3) are from unit C1 and C2, respectively. **b**, Locality map of the two sections based on ref. 3.

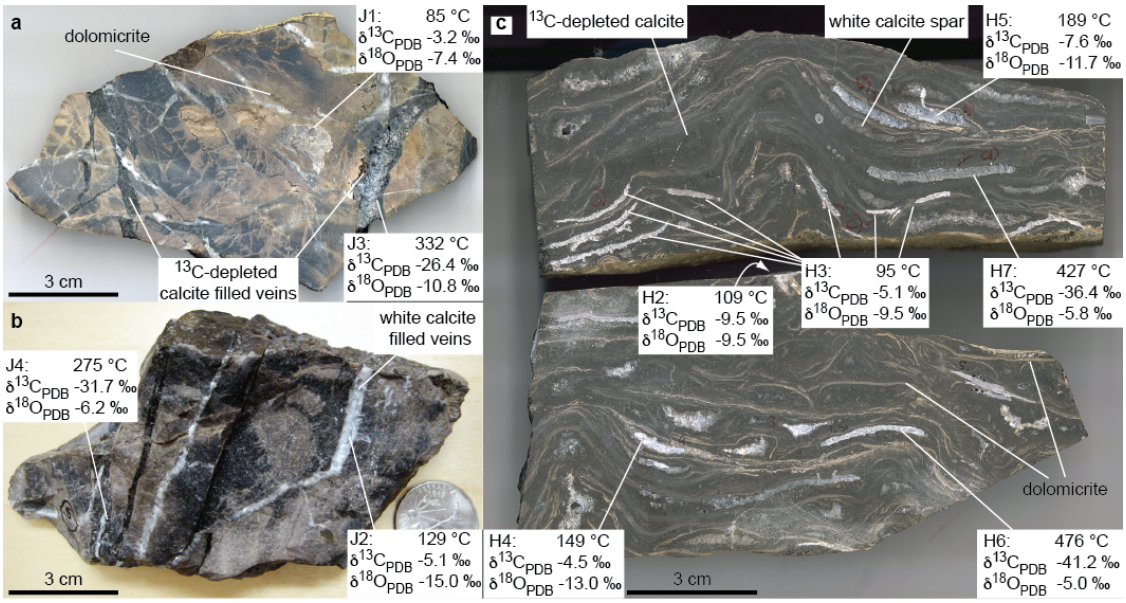

Supplementary Figure 2 | Scanned images of sample 1 (a and b) and 3 (c), with isotopic data and calculated temperatures. These are the same images shown in Fig. 1 of the main text, but highlighting of the sampling spots has been removed.

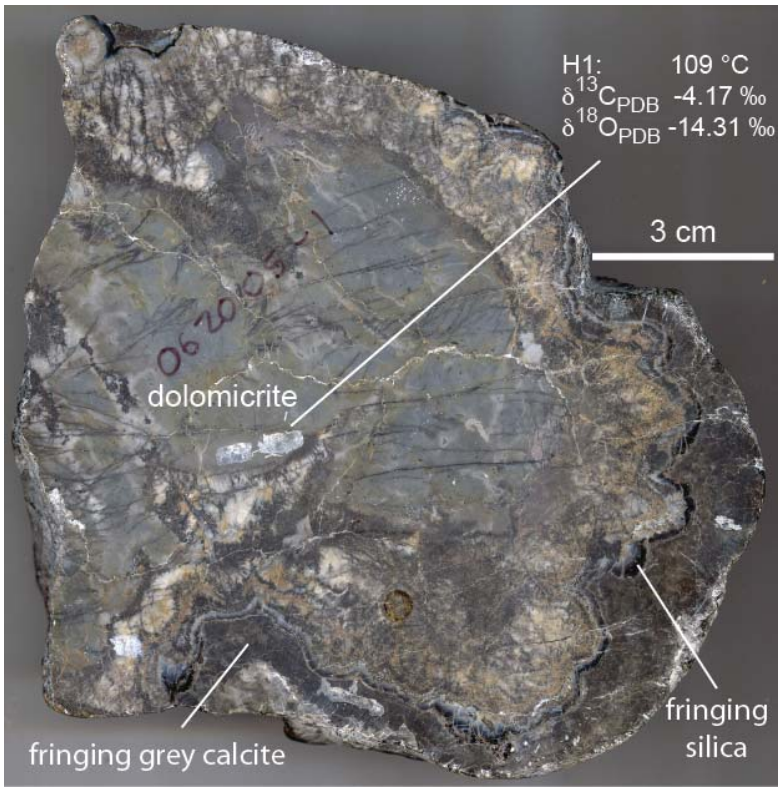

Supplementary Figure 3 | Scanned image of sample 2 showing the position of sampling spot H1.

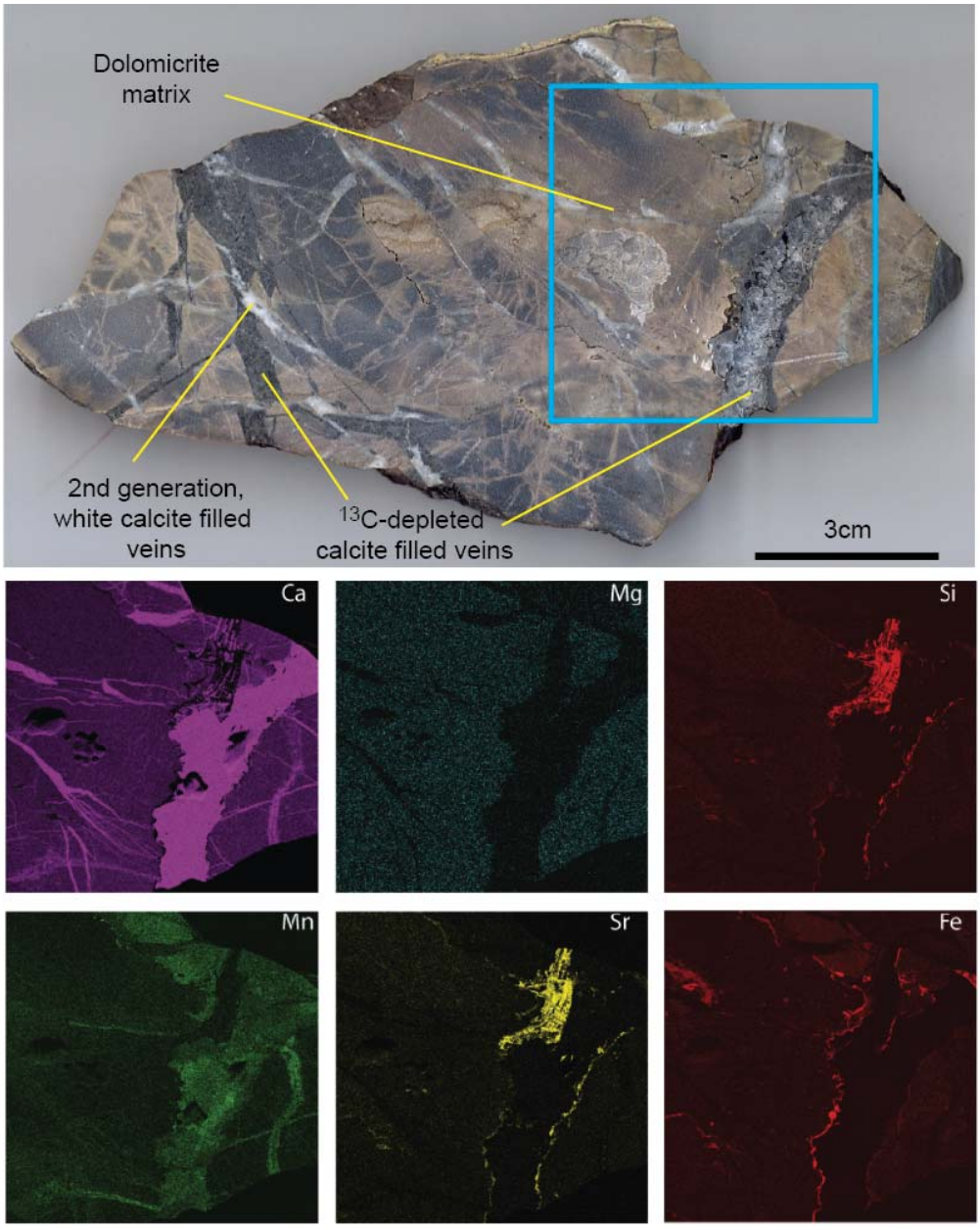

Supplementary Figure 4 | Scanned image (top panel) and elemental maps (made using the XRF scanner) of sample 1. Blue box shows area of elemental mapping. The various cements described in the main text are labelled.

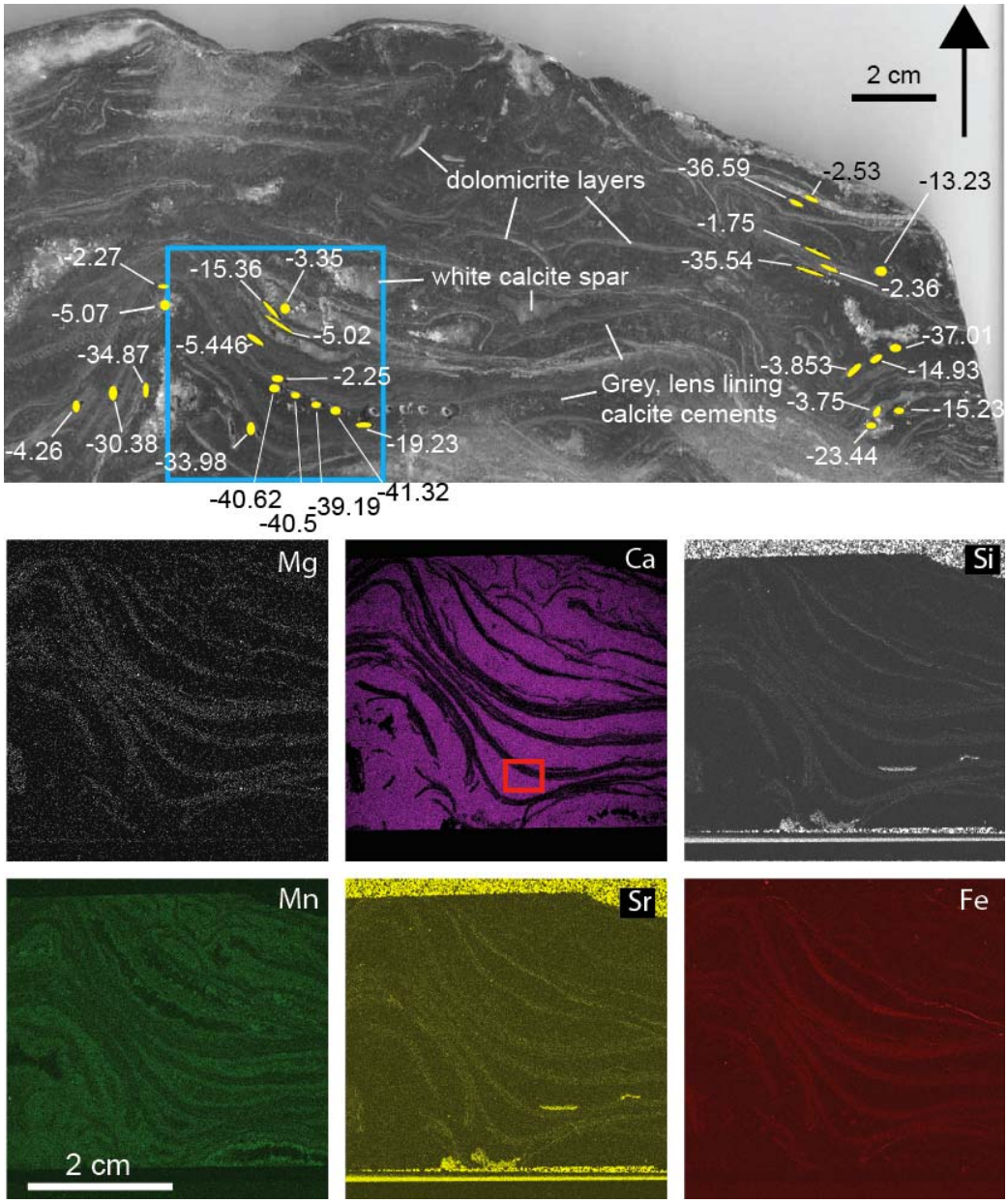

Supplementary Figure 5 | Scanned image (top panel) and elemental maps (made using the XRF scanner) of sample 3. Blue box in upper panel shows area of elemental mapping. The upper scanned image shows > 30‰ heterogeneity of $\delta^{13}C_{PDB}$ values of various cements at mm-scales (data from ref. 2). Red box in the Ca map shows the area mapped in finer detail with the electron microprobe shown in Supplementary Fig. 6.

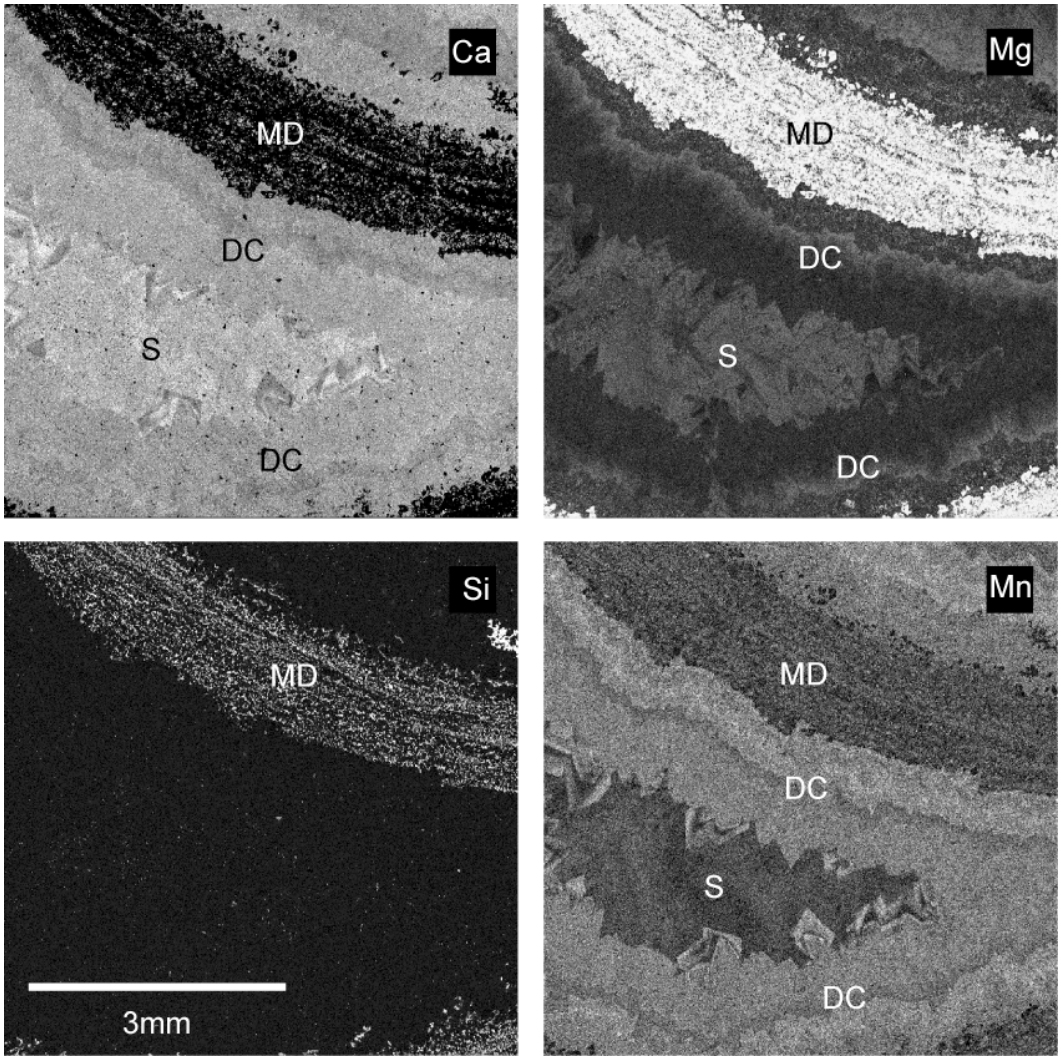

Supplementary Figure 6 | Elemental maps from the electron microprobe (Ca, Mg, Si and Mn) of part of sample 3 (see area outlined on Supplementary Fig. 5) showing three generations of carbonate cement. Lighter tones indicate higher concentration of the specified element. MD - silica cemented, dolomicrite layer, which is partially calcitized. DC - highly ^{13}C-depleted grey calcite. S - late void-filling white calcite spar. Highly ^{13}C-depleted calcite is the most enriched in Mn and depleted in Sr (see Supplementary Table 2 for spot analysis of cements).

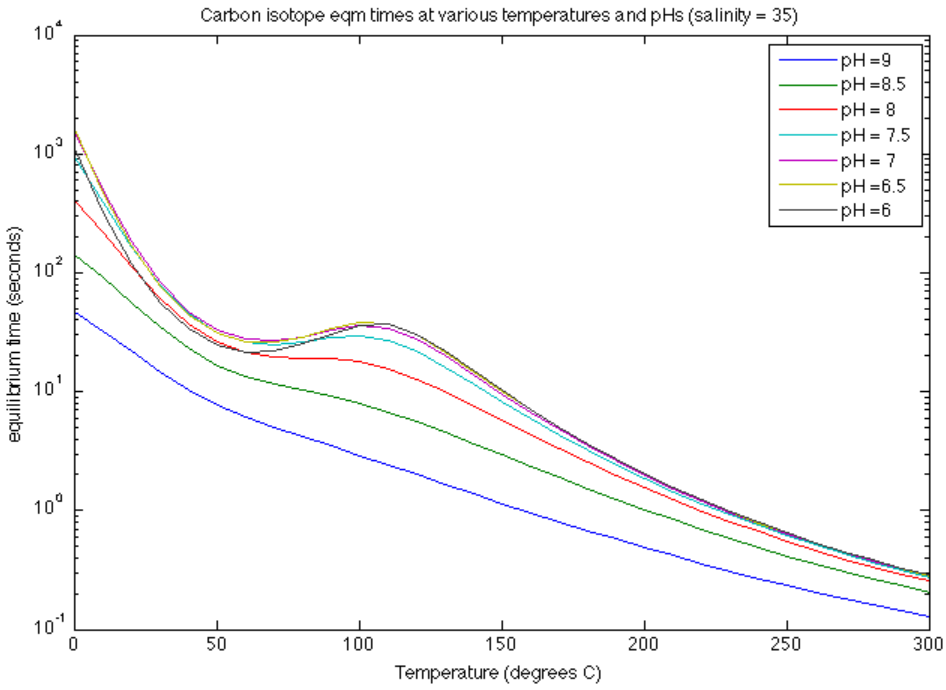

Supplementary Figure 7 | Temperature and pH dependence of the time needed to reach isotopic equilibrium in the carbonate system. Calculations are based on the equations described in ref. 25.

Supplementary Table 1 | Stable isotopes and temperature data from cap dolostone samples.

Sample /spot*	Carbonate phase	$\delta^{13}C_C$ (‰, PDB)	$\delta^{18}O_C$ (‰, PDB)	Δ_{47} (‰)	av. $\delta^{13}C_C$ (PDB)	±1σ	av. $\delta^{18}O_C$ (PDB)	±1σ	av. Δ_{47}	±1σ	av.T (°C)	±1σ	av. $\delta^{18}O_w$ (SMOW)	±1σ
Jiulongwan section														
1-J1	dolomicrite	-3.29	-8.00	0.49	**-3.22**	0.10	-7.36	0.90	0.487	0.003	**86**	5	1.7	1.3
1-J1	dolomicrite	-3.16	-6.72	0.49										
1-J2	white calcite spar	-5.08	-15.20	0.39										
1-J2	white calcite spar	-4.99	-14.91	0.45	**-5.02**	0.05	-14.99	0.19	0.421	0.027	**129**	8	11.3	0.3
1-J2	white calcite spar	-5.00	-14.85	0.42										
1-J3	^{13}C-depleted grey calcite	-26.27	-10.96	0.30										
1-J3	^{13}C-depleted grey calcite	-26.50	-10.61	0.27	**-26.40**	0.12	-10.77	0.18	0.292	0.018	**332**	36	18.0	0.6
1-J3	^{13}C-depleted grey calcite	-26.45	-10.74	0.30										
1-J4	^{13}C-depleted grey calcite	-32.02	-6.29	0.32										
1-J4	^{13}C-depleted grey calcite	-31.78	-6.05	0.31	**-31.72**	0.33	-6.18	0.12	0.311	0.010	**275**	27	22.3	0.3
1-J4	^{13}C-depleted grey calcite	-31.36	-6.20	0.30										
Huajipo section														
2-H1	dolomicrite	-4.19	-14.96	0.39	**-4.17**	0.04	-14.31	0.92	0.390	0.006	**156**	10	1.8	0.4
2-H1	dolomicrite	-4.14	-13.65	0.39										
3-H2	dolomicrite	-9.68	-9.98	0.45	**-9.49**	0.27	-9.46	0.72	0.446	0.003	**110**	5	2.4	1.0
3-H2	dolomicrite	-9.30	-8.95	0.44										
3-H3	dolomicrite	-5.27	-9.95	0.47	**-5.13**	0.20	-9.47	0.67	0.469	0.004	**95**	6	0.6	0.9
3-H3	dolomicrite	-4.99	-9.00	0.47										
3-H4	white calcite spar	-4.58	-13.03	0.39										
3-H4	white calcite spar	-4.23	-13.07	0.42	**-4.48**	0.22	-13.04	0.03	0.397	0.022	**149**	9	13.7	0.4
3-H4	white calcite spar	-4.63	-13.01	0.38										
3-H5	white calcite spar	-7.43	-11.70	0.35										
3-H5	white calcite spar	-7.62	-11.68	0.37	**-7.59**	0.15	-11.69	0.01	0.361	0.014	**189**	14	15.6	0.2
3-H5	white calcite spar	-7.72	-11.70	0.36										
3-H6	^{13}C-depleted grey calcite	-40.36	-5.10	0.29										
3-H6	^{13}C-depleted grey calcite	-41.68	-4.90	0.24	**-41.22**	0.75	-5.03	0.11	0.265	0.029	**476**	77	24.7	1.0
3-H6	^{13}C-depleted grey calcite	-41.63	-5.08	0.27										
3-H7	^{13}C-depleted grey calcite	-36.53	-5.67	0.27	**-36.35**	0.25	-5.75	0.11	0.266	0.005	**427**	61	23.8	0.0

3-H7	^{13}C-depleted grey calcite	-36.17	-5.83	0.26

$\delta^{13}C_C$ and $\delta^{18}O_C$ are the carbon and oxygen isotope compositions (relative to PDB) of cap dolostone samples. Δ_{47} is the difference in measured 47/44 ratios from the stochastic distribution based on the bulk stable carbon and oxygen isotope composition of that sample. T is the temperature in °C calculated from Δ_{47} (see Methods). $\delta^{18}O_W$ is the calculated oxygen isotope composition of fluid (relative to SMOW) in equilibrium with carbonate at the estimated temperature (see Methods). av. = mean of several independent measurements on the same powder and 1σ is one standard deviation , *the position of sample spots are shown in Fig. 1 of the main text and Supplementary Fig. 2 and 3. It is worth noting that in general highly ^{13}C-depleted calcite has the least reproducible ™$^{13}C_{PDB}$ measurements (on average ± 0.36‰) relative to other type of samples (on average ± 0.15‰). This probably indicates the introduction of minor contamination from other carbonate phases when powders were drilled.

Supplementary Table 2 | Trace element chemistry of carbonate phases from cap dolostone sample 3, determined using the electron microprobe.

		Fe (ppm)		Mn (ppm)		Sr (ppm)	
Carbonate Phase	n	Mean	Range	Mean	Range	Mean	Range
white calcite spar	11	511	b.d to 1,774	9,204	2,337 to 20,443	104	b.d to 486
^{13}C-depleted calcite	13	350	b.d to 1,549	12,141	2,142 to 20,628	109	b.d to 379
dolomicrite	7	4,378	1,027 to 6,761	5,773	1,815 to 8,399	190	b.d to 549
calcitized areas in dolomicrite	4	674	478 to 773	6,898	1,810 to 10,864	b.d	

n = number of spots analyzed
b.d = below detection

Supplementary Table 3 | Sr ratios of specific carbonate phases from cap dolostone samples 1 and 3.

Carbonate phase	^{87}Sr/^{86}Sr
Sample 1 (Jiulongwan)	
dolomicrite	0.70901
white calcite spar	0.71297
^{13}C-depleted grey calcite	0.70973
Sample 3 (Huajipo)	
dolomicrite layer	0.70982
white calcite spar	0.70990
^{13}C-depleted grey calcite	0.70963*

* average of two measurements

Supplementary Table 4 | Trace elements chemistry of carbonate phases with $\delta^{13}C_{PDB}$ values <-30‰ from modern and ancient cold seeps

Location	Phase	Method	Mn (ppm)	Sr (ppm)	Fe (ppm)	Ref.
Modern						
Black Sea	botryoidal aragonite	Probe	77	8903	78	26
	micritic Mg-calcite		465	1187	777	
Congo	various crusts and concretions	XRF	126	3059	6574	27
Monterey Bay, California	fine-grained calcite (#6)	Probe	b.d.	1438	5752	28
	proto-dolomite		77	1860	2643	
	ground-mass calcite (#14)		542	3805	389	
Holocene methane derived, dolomite cemented sandstone pillars, Denmark	equicrystalline dolomite	Probe	320	1015	1870	29
	high Mg calcite		230	350	2180	30
	aragonite		310	9600	390	
Ancient						
Upper Jurassic seep from Antarctica	laminated cement crust	Probe	b.d. to 320	640	b.d to 540	31
	microspar cement in geopetal fill		260 to 5400	50 to 530	310 to 2410	
	void filling spar		b.d. to 640	800	b.d. to 580	
Tantes Mound, Early Carboniferous, France	isopachous fibrous cement	ICP-AES	17	7611	81	32
	scalenohedral		1420	780	4830	

All metal concentrations are averages of multiple analyses, unless expressed as a range.
b.d. = below detection limit

Supplementary Table 5 | Sr isotope values of cold seep carbonates compared with contemporaneous seawater

Location	Phase	$^{87}Sr/^{86}Sr$ carbonate	$^{87}Sr/^{86}Sr$ seawater	Ref.
Modern cold seep carbonates - Black Sea	botryoidal aragonite	0.70918	0.70917	26
	micritic Mg-calcite	0.70927	0.70917	
Recent cold seep - Sea of Okhotsk	authigenic carbonates	0.70826 to 0.708722	0.7091	33
Methane related carbonate cements in North Sea	aragonite botryoids	0.70917	0.70917	34
	acicular aragonite cement	0.70915	0.70917	

Supplementary Notes

1. Jiang, G. Q., Kennedy, M. J. & Christie-Blick, N. Stable isotopic evidence for methane seeps in Neoproterozoic postglacial cap carbonates. *Nature* **426**, 822-826 (2003).

2. Jiang, G. Q., Kennedy, M. J., Christie-Blick, N., Wu, H. C. & Zhang, S. H. Stratigraphy, sedimentary structures, and textures of the late Neoproterozoic Doushantuo cap carbonate in south China. *J. Sediment. Res.* **76**, 978-995 (2006).

3. Wang, J. S., Jiang, G. Q., Xiao, S. H., Li, Q. & Wei, Q. Carbon isotope evidence for widespread methane seeps in the ca. 635 Ma Doushantuo cap carbonate in south China. *Geology* **36**, 347-350 (2008).

4. Bristow, T. F. *et al.* Mineralogical constraints on the paleoenvironments of the Ediacaran Doushantuo Formation. *Proc. Natl. Acad. Sci. USA* **106**, 13190-13195 (2009).

5. Fairchild, I. J. & Kennedy, M. J. Neoproterozoic glaciation in the Earth System. *J. Geol. Soc.* **164**, 895-921 (2007).

6. Hoffman, P. F. & Schrag, D. P. The snowball Earth hypothesis: testing the limits of global change. *Terra Nova* **14**, 129-155 (2002).

7. Eiler, J. M. & Schauble, E. $^{18}O^{13}C^{16}O$ in Earth's atmosphere. *Geochim. Cosmochim. Acta* **68**, 4767-4777 (2004).

8. Campbell, K. A. Hydrocarbon seep and hydrothermal vent paleoenvironments and paleontology: Past developments and future research directions. *Paleogeogr. Paleoclimatol. Paleoecol.* 232, 362-407 (2006).

9. Ghosh, P. *et al.* ^{13}C-^{18}O bonds in carbonate minerals: a new kind of paleothermometer. *Geochim. Cosmochim. Acta* **70**, 1439-1456 (2006).

10. Guo, W., Daëron, M., Niles, P., Goddard, W. & Eiler, J. M. Isotopic fractionations associated with degassing of CO_2 from aqueous solutions: implications for carbonate clumped isotope thermometry. *Geochim. Cosmochim. Acta* (in revision).

11. Shields, G. A. Neoproterozoic cap carbonates: a critical appraisal of existing models and the plumeworld hypothesis. *Terra Nova* **17**, 299-310 (2005).

12. Jacobson, S. B. & Kaufman, A. J. The Sr, C and O isotopic evolution of Neoproterozoic seawater. *Chem. Geol.* **161**, 37-57 (1999).

13. Halverson, G. P., Dudas, F. O., Maloof, A. C. & Bowring, S. A. Evolution of the Sr-87/Sr-86 composition of Neoproterozoic seawater. *Paleogeogr. Paleoclimatol. Paleoecol.* **256**, 103-129 (2007).

14. Kaufman, A. J. & Knoll, A. H. Neoproterozoic variations in the C-isotope composition of seawater: stratigraphic and biogeochemical implications. *Precam. Res.* **73**, 27-49 (1995).

15. Sawaki, Y. *et al.* The Ediacaran radiogenic Sr isotope excursion in the Doushantuo Formation in the Three Gorges area, South China. *Precam. Res.* **176**, 46-64 (2010).

16. Meunier, A. *Clays*. (Springer, 2005).

17. Chen, D., Wang, J., Qing, H., Yan, D. & Li, R. Hydrothermal venting activities in the Early Cambrian, South China: Petrological geochronological and stable isotopic constraints. *Chem. Geol.* **258**, 168-181 (2009).

18. Mao, J. *et al.* Re-Os dating of polymetallic Ni-Mo-PGE-Au mineralization in Lower Cambrian black shales of South China and its geologic significance. *Econ. Geol.* **97**, 1051–1061 (2002).

19. Lehman, B. *et al.* Highly metalliferous carbonaceous shale and Early Cambrian seawater. *Geology* **35**, 403–406 (2007).

20. Pašava, J. *et al.* Multiple Sources of Metals of Mineralization in Lower Cambrian Black Shales of South China: Evidence from Geochemical and Petrographic Study. *Res. Geol.* **58**, 25-42 (2007).

21. Jiang, S.Y. *et al.* Trace- and rare-earth element geochemistry and Pb-Pb dating of black shales and intercalated Ni-Mo-PGE-Au sulfide ores in Lower Cambrian strata: Yangtze Platform: South China. *Mineralium Deposita* **41**, 453–468 (2006).

22. Lott, D.A., Conveney Jr., R.M., Murowichick, J.B. & Grauch, R.I. Sedimentary exhalative nickel–molybdenum ores in south China. *Econ. Geol.* **94**, 1051–1066 (1999).

23. Wang, M., Sun, X. & Ma, M. Microthermometric measurement of fluid inclusions and its constraints on genesis of PGE-polymetallic deposits in Lower Cambrian black rock series, southern China. *Chinese J. Geochem.* **24**, 297- 305 (2005).

24. Belkin, H. E. & Luo, K. Late-stage sulfides and sulfarsenides in Lower Cambrian black shale (stone coal) from the Huangjiawan mine, Guizhou Province, People's Republic of China. *Min. Petrol.* **92**, 321-340 (2008).

25. Zeebe, R.E. & Wolf-Gladrow, D. *CO_2 in seawater: equilibrium, kinetics, isotopes*. (Elsevier, 2001).

26. Peckmann, J. *et al.* Methane-derived carbonates and authigenic pyrite from the northwestern Black Sea. *Mar. Geol.* **177**, 129-150 (2001).

27. Pierre, C. & Fouquet, Y. Authigenic carbonates from methane seeps of the Congo deep-sea fan. *Geo-Mar. Lett.* **27**, 249-257 (2007).

28. Stakes, D. S., Orange, D., Paduan, J. B., Salamy, K. A. & Maher, N. Cold-seeps and authigenic carbonate formation in Monterey Bay, California. *Mar. Geol.* **159**, 93-109 (1999).

29. Jorgensen, N. O. Holocene methane-derived, dolomite-cemented sandstone pillars from the Kattegat, Denmark. *Mar. Geol.* **88**, 71-81 (1989).

30. Jorgensen, N. O. Methane-derived carbonate cementation of holocene marine-sediments from Kattegat, Denmark. *Cont. Shelf Res.* **12**, 1209-1218 (1992).

31. Kelly, S. R. A., Ditchfield, P. W., Doubleday, P. A. & Marshall, J. D. An Upper Jurassic methane-seep limestone from the Fossil Bluff Group fore-arc basin of Alexander Island, Antarctica. *J. Sediment. Res.* **65**, 274-282 (1995).

32. Buggisch, W. & Krumm, S. Palaeozoic cold seep carbonates from Europe and North Africa - an integrated isotopic and geochemical approach. *Facies* **51**, 585-602 (2005).

33. Greinert, J., Bollwerk, S. M., Derkachev, A., Bohrmann, G. & Suess, E. Massive barite deposits and carbonate mineralization in the Derugin Basin, Sea of Okhotsk: precipitation processes at cold seep sites. *Earth Planet. Sci. Lett.* **203**, 165-180 (2002).

34. Hovland, M., Talbot, M. R., Qvale, H., Olaussen, S. & Aasberg, L. Methane-related carbonate cements in pockmarks of the North Sea *J. Sed. Petrol.* **57**, 881-892 (1987).